

Cite this: *Chem. Commun.*, 2019, 55, 6377Received 19th March 2019,
Accepted 7th May 2019

DOI: 10.1039/c9cc02174d

rsc.li/chemcomm

An exceptionally stable core–shell MOF/COF bifunctional catalyst for a highly efficient cascade deacetalization–Knoevenagel condensation reaction†

Ming-Liang Gao,[‡] Mei-Hong Qi,[‡] Lin Liu* and Zheng-Bo Han[‡]*

A novel strategy has been developed to construct a highly stable core–shell MOF@COF (PCN-222-Co@TpPa-1) bifunctional catalyst through strong π – π stacking interaction. This hybrid material with spatially isolated antagonistic acid–base sites can effectively catalyze the deacetalization–Knoevenagel condensation cascade reaction.

Multifunctional nanocrystalline catalysts, with two or more functional active sites integrated into one system, have gained a great deal of attention owing to their highly efficient activity for one-pot cascade reactions.¹ Multifunctional catalyst-participated cascade reactions not only show high atom-economy and are energy-saving and low-cost, but also provide an intriguing direction for complex organic synthesis.² However, the design and fabrication of multifunctional catalysts with precise isolation of antagonistic acid–base groups to achieve catalytic activity are probably the main reasons that limit cascade reactions.³

Metal–organic frameworks (MOFs) composed of metal ions and organic linkers have received increasing attention in recent years.⁴ Owing to their long-range ordered porous structure, high specific surface area and excellent chemical and thermal stability, MOFs present promising application in gas storage and separation, drug delivery, heterogeneous catalysis and so on.⁵ Similarly, covalent organic frameworks (COFs), as a class of promising porous crystalline polymers, are also receiving increasing attention due to their outstanding inherent properties, such as high surface area, tuneable pore size, and adjustable frameworks.⁶ COFs, based on reticular chemistry, are constructed from light elements (*e.g.*, C, N, B, and O) by strong covalent linkages and have shown great potential in various applications.⁷ Recently, core–shell MOF/COF hybrid materials have been developed and still remain largely unexplored.^{8–12} Zhang and co-workers developed an NH₂-MIL-68@TPA-COF core–shell hybrid material which was

utilized as an effective photo-catalyst for the degradation of organic pollutants.⁹ The Kim group reported a Pd/TiATA@LZU1 hybrid material which showed fascinating photocatalytic performance.¹⁰ Lan *et al.* reported NH₂-UiO-66/TpPa-1-COF hybrid materials for photocatalytic H₂ evolution.¹¹ Zhao and co-workers fabricated mixed matrix membranes containing NH₂-UiO-66/TpPa-1 hybrid fillers for efficient CO₂/CH₄ separation.¹² All the above core–shell MOF@COF hybrid materials were used in the same synthetic strategy which utilized amino-functionalized MOFs to graft with imine-based COFs. Though the enormous efforts are being spent on preparing the composite of MOFs and COFs, the universality of this strategy is restrained because amino-functionalized MOFs are fewer than the common MOFs. Therefore, to develop a general strategy to construct MOF@COF hybrid materials is urgent. Interestingly, 2D COFs possess a strong π -electron system with many phenyl rings and planar structures, which also exist in MOF materials.¹³ Owing to the aromaticity of MOFs and the ordered π -columnar structure characteristics of COFs, strong π – π stacking interaction provides an opportunity to construct MOF@COF hybrid materials with tunable nature and function of the parent species. Therefore, it is anticipated that construction of core–shell MOF@COF hybrid materials could overcome their inherent weak points and create a synergistic effect to afford multifunctional properties for specific applications. To the best of our knowledge, MOF@COF hybrid materials with a unique core–shell structure, π – π stacking interaction, and sizable specific surface area have not yet been reported as bifunctional acid–base cascade catalysts.

Bearing the above points in mind, we proposed a novel strategy to construct well-defined and hierarchical MOF@COF hybrid materials through strong π – π stacking interaction. The as-synthesized core–shell PCN-222-Co@TpPa-1 simultaneously exhibits the features of PCN-222-Co and TpPa-1, including (i) Lewis acid active sites in PCN-222-Co (the Co(II) sites and the Zr(IV) clusters); (ii) Brønsted base active sites in TpPa-1 (imine groups); and (iii) strong interaction between the reactants and the core–shell PCN-222-Co@TpPa-1 hybrid material due to the π – π stacking interaction. For these reasons, PCN-222-Co@TpPa-1 can

College of Chemistry, Liaoning University, Shenyang 110036, P. R. China.

E-mail: ceshzb@lnu.edu.cn, liulin@lnu.edu.cn

† Electronic supplementary information (ESI) available: Experimental details of synthesis and catalysis, and additional characterization studies. See DOI: 10.1039/c9cc02174d

‡ These authors contributed equally to this work.



Scheme 1 The synthetic route of PCN-222-Co@TpPa-1.

act as a highly efficient bifunctional catalyst for one-pot cascade reactions. Impressively, core-shell PCN-222-Co@TpPa-1 exhibited high chemical and thermal stability, recyclability, and durable catalytic activity under mild conditions.

The core-shell PCN-222-Co@TpPa-1 was prepared by a simple route under room temperature conditions (Scheme 1). The PXRD pattern confirmed the crystalline structure of PCN-222-Co@TpPa-1 and showed good agreement with the corresponding simulated patterns of PCN-222-Co and TpPa-1. Furthermore, due to the weak intensity of TpPa-1, PCN-222-Co@TpPa-1 exhibited intense peaks similar to PCN-222-Co (Fig. S1a, ESI[†]).^{14a} Moreover, the FT-IR spectrum was used to characterize the composition of PCN-222-Co@TpPa-1. As displayed in Fig. S1b (ESI[†]), the obvious appearance of stretching bands was similar to both PCN-222-Co and TpPa-1.^{14b} The asymmetric and symmetric stretching vibrations of the carboxylate groups appeared at 1607 and 1418 cm^{-1} , respectively. It can be seen that two new characteristic adsorption bands in PCN-222-Co@TpPa-1 for C–N and C=C groups at 1271 cm^{-1} and 1584 cm^{-1} indicated the formation of TpPa-1, further proving the successful combination of PCN-222-Co and TpPa-1. In addition, the chemical stability of core-shell PCN-222-Co@TpPa-1 was investigated by soaking PCN-222-Co@TpPa-1 in different solvents including CH_3OH , pyridine, CH_2Cl_2 , DMSO, 1,4-dioxane, toluene, water, and even pH = 2 HCl aqueous solution for 24 h. The PXRD patterns after soaking in different solvents were the same as that of pristine PCN-222-Co@TpPa-1, confirming the chemical stability of the hybrid material (Fig. S1c, ESI[†]). Variable-temperature PXRD and thermogravimetric analysis (TGA) were also investigated and the results revealed that PCN-222-Co@TpPa-1 could be stable up to 300 $^\circ\text{C}$ in air (Fig. S1d and S2, ESI[†]). The UV-vis diffuse reflectance spectroscopy (DRS) spectra of PCN-222-Co, TpPa-1 and PCN-222-Co@TpPa-1 are shown in Fig. S3 (ESI[†]). The main absorption peaks are located at about 498 and 572 nm for PCN-222-Co and PCN-222-Co@TpPa-1, respectively. The large redshifts of 74 nm indicated the π - π stacking interaction between PCN-222-Co and TpPa-1 in PCN-222-Co@TpPa-1.¹⁵

Scanning electron microscopy (SEM) and transmission electron microscopy (TEM) were performed to evaluate the morphologies of PCN-222-Co, TpPa-1, and PCN-222-Co@TpPa-1. Fig. 1a shows that the as-synthesized PCN-222-Co has an ellipsoid shape with a smooth surface and a uniform average size of 380 ± 20 nm and width of 200 ± 20 nm. As shown in Fig. 1b, the bare TpPa-1

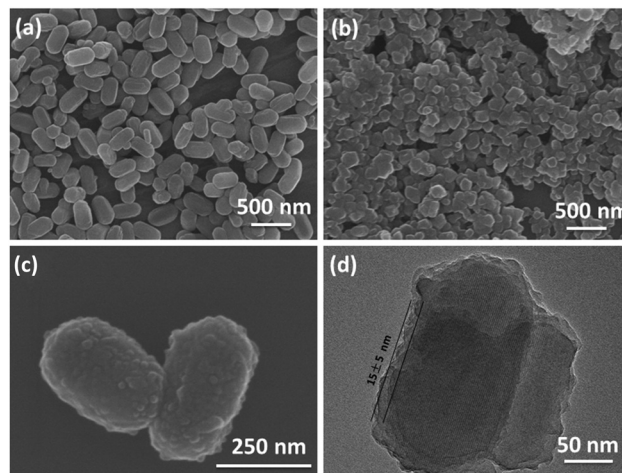


Fig. 1 The SEM images of (a) PCN-222-Co; (b) TpPa-1; (c) PCN-222-Co@TpPa-1; and (d) the TEM image of PCN-222-Co@TpPa-1.

possesses a plate-like morphology with a regular shape. In addition, TpPa-1 shells of different thicknesses were constructed: the thin TpPa-1 shell denoted as PCN-222-Co@TpPa-1(thin) and the thick TpPa-1 shell denoted as PCN-222-Co@TpPa-1(thick). The SEM images of PCN-222-Co@TpPa-1, PCN-222-Co@TpPa-1(thin) and PCN-222-Co@TpPa-1(thick) revealed that the smooth surface of pristine PCN-222-Co became rough, but the morphology of PCN-222-Co was well retained (Fig. 1c and Fig. S4, ESI[†]). The TEM images of PCN-222-Co@TpPa-1 demonstrated that TpPa-1 uniformly distributed on the surface of PCN-222-Co and the thickness of TpPa-1 was 15 ± 3 nm (Fig. 1d). As shown in Fig. S5 (ESI[†]), the TpPa-1 shell in PCN-222-Co@TpPa-1(thin) was about 3.2 nm and the aggregation of PCN-222-Co@TpPa-1(thick) was observed. SEM and TEM confirmed the successful preparation of the core-shell PCN-222-Co@TpPa-1.

N_2 adsorption-desorption experiments at 77 K were carried out for PCN-222-Co, TpPa-1 and core-shell PCN-222-Co@TpPa-1 to evaluate their permanent porosity characteristics (Fig. S6, ESI[†]). A typical type-IV isotherm of PCN-222-Co was obtained and exhibited a steep increase at the point of $P/P_0 = 0.2$ corresponding to the mesoporous channel of 3.7 nm in PCN-222 with a Brunauer-Emmett-Teller (BET) specific surface area of $2027 \text{ m}^2 \text{ g}^{-1}$.¹⁶ The TpPa-1 absorption isotherm showed a typical type-I isotherm, suggesting microporosity and a BET surface area of $632 \text{ m}^2 \text{ g}^{-1}$.¹⁷ The BET surface area of PCN-222-Co@TpPa-1 is $981 \text{ m}^2 \text{ g}^{-1}$, which is higher than that of pure TpPa-1 due to the presence of PCN-222-Co in the core of the hybrid material.

The Knoevenagel condensation reaction is well-known, not only as a base-catalyzed model reaction but also as an important C–C bond-forming reaction in organic synthesis for the preparation of coumarins and their derivatives, which are important intermediates in the synthesis of cosmetics, perfumes and pharmaceuticals. But, the aromatic aldehydes as the reactants of the Knoevenagel condensation reaction were easily oxidized under ambient conditions. Therefore, one-pot deacetalization-Knoevenagel condensation cascade reaction sequences were extensively investigated for the past few years. On the basis of PCN-222-Co@TpPa-1

possessing separate antagonistic catalytic sites, PCN-222-Co@TpPa-1 was used as an acid–base bifunctional catalyst to catalyze a one-pot cascade deacetalization–Knoevenagel condensation reaction. The one-pot cascade reaction can be considered to have two sequential steps: first, the unsaturated Zr(IV) and Co(II) centres catalyzed benzaldehyde dimethylacetal to generate benzaldehyde; second, the imine groups in TpPa-1 catalyzed the Knoevenagel condensation reaction to produce 2-benzylidenemalononitrile. Typically, the deacetalization–Knoevenagel condensation reaction was performed with benzaldehyde dimethylacetal (0.1 mmol) and malononitrile (0.11 mmol) in DMSO-*d*₆ (2.0 mL) under an N₂ atmosphere at 50 °C for 10 h. The conversion and yield were monitored by ¹H NMR spectroscopy based on the starting reactants and the results are listed in Table 1. As expected, the result showed that the one-pot cascade reaction can be efficiently catalyzed by core–shell PCN-222-Co@TpPa-1 with a high yield of 99.3% (Table 1, entry 1). More interestingly, the cascade reaction did not require the addition of extra water, probably owing to the presence of trace water in the organic solvent or the successive production of water in the second step of the cascade reaction sequence. Compared with the other reported catalysts, such as Yb-BCD-NH₂, LZSM-5-AT-OH[−] and PCN-124, PCN-222-Co@TpPa-1 exhibited the best catalytic activity for the deacetalization–Knoevenagel reaction (Table 1, entries 2–4).

To better understand the catalytic activity of PCN-222-Co@TpPa-1, control experiments were investigated. The product could not be observed when no catalyst was added into the reaction system (Table 1, entry 5). PCN-222-Co could efficiently catalyze the first step reaction (acid-catalyzed deacetalization reaction) to obtain intermediate product benzaldehyde with a

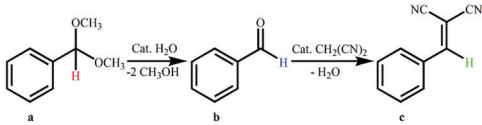
yield of 98.7%, but could not convert benzaldehyde to 2-benzylidenemalononitrile (Table 1, entry 6). TpPa-1 could not catalyze the cascade reaction due to the lack of Lewis acid active sites (Table 1, entry 7). Compared with PCN-222-Co@TpPa-1, the yield of the target product was low when using PCN-222@TpPa-1 as a catalyst (Table 1, entry 8). As the porphyrin linkers were metallized with Co(II) ions, Lewis acid sites of PCN-222-Co were much richer than those of PCN-222. The increase of catalytic activity was attributed to the presence of dual Lewis acid sites.¹⁹ Compared with core–shell PCN-222-Co@TpPa-1, 83.9% yield of 2-benzylidenemalononitrile was achieved by the physical mixture of PCN-222-Co and TpPa-1 with identical concentrations of catalytic sites (Table 1, entry 9). The reason was attributed to the entry of benzaldehyde dimethylacetal into the PCN-222-Co core to produce benzaldehyde, and then the formed benzaldehyde can immediately be activated by the TpPa-1 shell and react with malononitrile to generate target products. However, the cascade reaction cannot proceed smoothly when using a physical mixture catalyst as expected, because a part of benzaldehyde can escape from PCN-222-Co directly without further reaction on TpPa-1.

Moreover, the catalytic performance of PCN-222-Co@TpPa-1(thin) and PCN-222-Co@TpPa-1(thick) was investigated. When using PCN-222-Co@TpPa-1(thin) as a catalyst, the conversion of benzaldehyde dimethylacetal was 98.6%, but the yields of benzaldehyde and 2-benzylidenemalononitrile were 17.8% and 80.8%, respectively, which could be ascribed to a relatively small number of base sites (Table 1, entry 10). In addition, the catalytic activity of PCN-222-Co@TpPa-1(thick) was lower than that of PCN-222-Co@TpPa-1, and the yield of 2-benzylidenemalononitrile was 75.2% because a mass of TpPa-1 partially blocks the reactants' entry into the pores of the PCN-222-Co catalyst (Table 1, entry 11).

In detail, the kinetic investigation revealed that the reaction completed within 10 h (Fig. S7, ESI†). During the reaction, PCN-222-Co@TpPa-1 did not leach with no detection of Co and Zr ions in the filtrate as measured by ICP-OES and no other active substance was retained in the isolated solution (Fig. S8a, ESI†).²⁰ In addition, the recyclability of PCN-222-Co@TpPa-1 was investigated after the catalyst was recovered from the cascade reaction through centrifugation. The catalytic activity of the catalyst showed no obvious decrease within 5 runs (Fig. S8b, ESI†). Furthermore, PXRD and FT-IR revealed that the crystallinity and structural integrity of PCN-222-Co@TpPa-1 were remained even after 5 cycles, indicating its excellent stability (Fig. S9a and b, ESI†). After the 5th cycle, the porosity of PCN-222-Co@TpPa-1 were remained, which was confirmed by N₂ adsorption–desorption experiments at 77 K and a BET surface area of 898 m² g^{−1} (Fig. S10, ESI†). The SEM image of core–shell PCN-222-Co@TpPa-1 after cycling tests revealed that its morphology remains unchanged (Fig. S11, ESI†).

In conclusion, a general strategy has been developed to construct core–shell MOF@COF hybrid materials by employing strong π – π stacking interaction. The core–shell PCN-222-Co@TpPa-1 with both Lewis acid sites (Co(II) sites and the Zr(IV) clusters) and Brønsted base active sites in TpPa-1 (imine groups), which showed high chemical and thermal stability, was prepared for the first time. In addition, the core–shell PCN-222-Co@TpPa-1 was used to catalyze the one-pot deacetalization–Knoevenagel

Table 1 One-pot cascade deacetalization–Knoevenagel condensation reaction monitored by ¹H NMR^a



| Entry | Catalyst | Conv. of a (%) | Yield of b (%) | Yield of c (%) |
|-------|-------------------------------------|----------------|----------------|----------------|
| 1 | PCN-222-Co@TpPa-1 | 99.3 | Trace | 99.3 |
| 2 | Yb-BCD-NH ₂ ^b | 97.0 | Trace | 97.0 |
| 3 | LZSM-5-AT-OH ^{−c} | 98.5 | 7.3 | 91.2 |
| 4 | PCN-124 ^d | 99 | — | 99 |
| 5 | No catalyst | Trace | Trace | Trace |
| 6 | PCN-222-Co | 98.7 | 91.7 | 6.0 |
| 7 | TpPa-1 | Trace | Trace | Trace |
| 8 | PCN-222@TpPa-1 | 47.6 | Trace | 47.6 |
| 9 | PCN-222-Co + TpPa-1 | 99.1 | 15.2 | 83.9 |
| 10 | PCN-222-Co@TpPa-1(thin) | 98.6 | 17.8 | 80.8 |
| 11 | PCN-222-Co@TpPa-1(thick) | 75.2 | Trace | 75.2 |

^a Reaction conditions: benzaldehyde dimethylacetal (0.1 mmol), malononitrile (0.11 mmol), DMSO-*d*₆ (2 mL) and catalyst (5 mg); reaction temperature: 50 °C; reaction time: 10 h. ^b Benzaldehyde dimethylacetal (2 mmol), malononitrile (2.1 mmol) and DMSO-*d*₆ (2 mL), catalyst (100 mg), 50 °C and 24 h. ^{18a} ^c Benzaldehyde dimethylacetal (5 mmol), malononitrile (5 mmol), acetonitrile (2 mL), H₂O, (20 μg), catalyst (50 mg), 80 °C, 15 h. ^{18b} ^d Benzaldehyde dimethylacetal (2 mmol), malononitrile (2.1 mmol), PCN-124 (0.01 mmol), DMSO-*d*₆ (2 mL), 50 °C, 12 h.^{18c}

condensation cascade reaction with high catalytic activity (yield of 99.3%) and good recyclability. This strategy would be extensively employed in the development of functional MOF hybrid materials and high performance heterogeneous catalysts that can be applied in cascade reactions.

We thank the National Natural Science Foundation of China for its financial support (21671090 and 21701076) and Liaoning Province Doctor Startup Fund (20180540056).

Conflicts of interest

The authors declare no competing financial interest.

Notes and references

- (a) F. X. Felpin and E. Fouquet, *ChemSusChem*, 2008, **1**, 718–724; (b) M. J. Climent, A. Corma and S. Iborra, *Chem. Rev.*, 2010, **111**, 1072–1133.
- P. Li, C. Y. Cao, H. Liu, Y. Yu and W. G. Song, *J. Mater. Chem. A*, 2013, **1**, 12804–12810.
- (a) F. Gelman, J. Blum and D. Avnir, *Angew. Chem., Int. Ed.*, 2001, **40**, 3647–3649; (b) N. A. Brunelli, S. A. Didas, K. Venkatasubbaiah and C. W. Jones, *J. Am. Chem. Soc.*, 2012, **134**, 13950–13953.
- (a) H. Furukawa, K. E. Cordova, M. O’Keeffe and O. M. Yaghi, *Science*, 2013, **341**, 1230444; (b) T. Kitao, Y. Zhang, S. Kitagawa, B. Wang and T. Uemura, *Chem. Soc. Rev.*, 2017, **46**, 3108–3133; (c) N. Wei, Y. Zhang, L. Liu, Z. B. Han and D. Q. Yuan, *Appl. Catal., B*, 2017, **219**, 603–610; (d) M. L. Gao, W. J. Wang, L. Liu, Z. B. Han, N. Wei, X. M. Cao and D. Q. Yuan, *Inorg. Chem.*, 2017, **56**, 511–517.
- T. Rodenas, I. Luz, G. Prieto, B. Seoane, H. Miro, A. Corma, F. Kapteijn, F. X. Llabrés i Xamena and J. Gascon, *Nat. Mater.*, 2015, **14**, 48–55.
- (a) C. S. Diercks and O. M. Yaghi, *Science*, 2017, **355**, 1585; (b) N. Huang, P. Wang and D. Jiang, *Nat. Rev. Mater.*, 2016, **1**, 16068.
- S. Y. Ding and W. Wang, *Chem. Soc. Rev.*, 2013, **42**, 548–568.
- (a) Y. Mao, J. Li, W. Cao, Y. Ying, P. Hu, Y. Liu, L. Sun, H. Wang, C. Jin and X. Peng, *Nat. Commun.*, 2014, **5**, 5532; (b) D. Bradshaw, A. Garai and J. Huo, *Chem. Soc. Rev.*, 2012, **41**, 2344–2381; (c) K. Khaletskaia, J. Reboul, M. Meilikhov, M. Nakahama, S. Diring, M. Tsujimoto, S. Isoda, F. Kim, K. Kamei, R. A. Fischer, S. Kitagawa and S. Furukawa, *J. Am. Chem. Soc.*, 2013, **135**, 10998–11005; (d) N. Stock and S. Biswas, *Chem. Rev.*, 2012, **112**, 933–969; (e) J. Cortés-Suárez, V. Celis-Arias, H. I. Beltrán, A. Tejada-Cruz, I. A. Ibarra, J. E. Romero-Ibarra, E. Sánchez-González and S. Loera-Serna, *ACS Omega*, 2019, **4**, 5275–5282.
- Y. Peng, M. Zhao, B. Chen, Z. Zhang, Y. Huang, F. Dai, Z. Lai, X. Cui, C. Tan and H. Zhang, *Adv. Mater.*, 2018, **30**, 170545.
- D. Sun, S. Jang, S. J. Yim, L. Ye and D. P. Kim, *Adv. Funct. Mater.*, 2018, **28**, 1707110.
- F. M. Zhang, J. L. Sheng, Z. D. Yang, X. J. Sun, H. L. Tang, M. Lu, H. Dong, F. C. Shen, J. Liu and Y. Q. Lan, *Angew. Chem., Int. Ed.*, 2018, **57**, 12106–12110.
- Y. Cheng, Y. Ying, L. Zhai, G. Liu, J. Dong, Y. Wang, M. P. Christopher, S. Long, Y. Wang and D. Zhao, *J. Membr. Sci.*, 2019, **573**, 97–106.
- (a) J. Fu, S. Das, G. Xing, T. Ben, V. Valtchev and S. Qiu, *J. Am. Chem. Soc.*, 2016, **138**, 7673–7680; (b) X. Liu, M. Hu, M. Wang, Y. Song, N. Zhou, L. He and Z. Zhang, *Biosens. Bioelectron.*, 2019, **123**, 59–68.
- (a) T. He, X. Xu, B. Ni, H. Wang, Y. Long, W. Hua and X. Wang, *Nanoscale*, 2017, **9**, 19209–19215; (b) Y. Peng, W. K. Wong, Z. Hu, Y. Cheng, D. Yuan, S. A. Khan and D. Zhao, *Chem. Mater.*, 2016, **28**, 5095–5101.
- Q. Peng, X. Liu, D. Su, G. Fu, J. Xu and L. Dai, *Adv. Mater.*, 2011, **23**, 4554–4558.
- L. Li, Q. Yang, S. Chen, X. Hou, B. Liu, J. Lu and H. Jiang, *Chem. Commun.*, 2017, **53**, 10026–10029.
- L. Liu, W. K. Meng, Y. S. Zhou, X. Wang, G. J. Xu, M. L. Wang, J. M. Lin and R. S. Zhao, *Chem. Eng. J.*, 2019, **365**, 926–933.
- (a) Y. Zhang, Y. Wang, L. Liu, N. Wei, M. L. Gao, D. Zhao and Z. B. Han, *Inorg. Chem.*, 2018, **57**, 2193–2198; (b) L. Xu, C. Li, K. Zhang and P. Wu, *ACS Catal.*, 2014, **4**, 2959–2968; (c) J. Park, J. R. Li, Y. P. Chen, J. Yu, A. A. Yakovenko, Z. U. Wang, L. B. Sun, P. B. Balbuena and H. C. Zhou, *Chem. Commun.*, 2012, **48**, 9995–9997.
- J. Zhu, P. M. Usov, W. Xu, P. J. Celis-Salazar, S. Lin, M. C. Kessinger, C. Landaverde-Alvarado, M. Cai, A. M. May, C. Slebodnick, D. Zhu, S. D. Senanayake and A. J. Morris, *J. Am. Chem. Soc.*, 2018, **140**, 993–1003.
- K. Wang, Z. Jia, X. Yang, L. Wang, Y. Gu and B. Tan, *J. Catal.*, 2017, **348**, 168–176.